Optical Materials 111 (2021) 110717

Contents lists available at ScienceDirect

Optical Materials

journal homepage: http://www.elsevier.com/locate/optmat

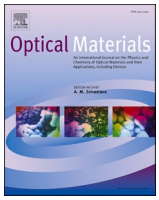

Effect of terbium and silver co-doping on the enhancement of photoluminescence in $CaSO_4$ phosphors

Anderson M.B. Silva [a], Wellisson S. Silveira [a], Tawany S. Matos [a], Danilo O. Junot [b,c], Marcos V. S. Rezende [a], Divanizia N. Souza [a,*]

[a] Departamento de Física, Universidade Federal de Sergipe; Marechal Rondon, S/N, 49.100-000, São Cristóvão, SE, Brazil
[b] Instituto de Pesquisas Energéticas e Nucleares, Comissão Nacional de Energia Nuclear, IPEN/CNEN-SP, Av. Prof. Lineu Preste, 2242, 05508-000, São Paulo, SP, Brazil
[c] Instituto de Física Armando Dias Tavares, Universidade do Estado do Rio de Janeiro UERJ, Rua São Francisco Xavier, 524, 20550-013, Rio de Janeiro, RJ, Brazil

ARTICLE INFO

Keywords:
$CaSO_4$
Terbium
Silver
Optical properties

ABSTRACT

In this work, the photoluminescence properties of $CaSO_4$ crystals co-doped with terbium and silver from silver oxide or silver nanoparticles (NPs) in different concentrations are investigated. Phosphors are obtained by means of a slow evaporation route and calcined at 600 °C for 1 h. X-ray diffraction analysis shows the formation of a single-phase anhydrite structure with orthorhombic symmetry. The photoluminescence properties are investigated using vacuum ultraviolet, ultraviolet and X-ray excitation. All luminescent measurements reveal the characteristic emissions of Tb^{3+}. The analyses using excitation with ultraviolet light show that the Ag NPs are able to generate structural defects more satisfactorily compared to $CaSO_4$:Tb with silver oxide. We also observe that higher concentrations of Ag increase the Tb^{3+} emission intensity, while higher concentrations of Ag NPs decrease it. The good stability of $CaSO_4$ results in an efficient energy transfer from the host lattice to the activator under X-ray excitation, with the NPs contributing to the increase in luminescent intensity. Investigation of the terbium valence in the $CaSO_4$ host shows a complete reduction of the Tb^{4+} present in Tb_4O_7 to Tb^{3+}, as indicated by the X-ray absorption near edge structure. The vacuum ultraviolet excitation spectra reveal three broad bands, attributed to the charge-transfer excitations within SO_4^{2-} complexes and to the $4f^8 \rightarrow 4f^7 5d^1$ transitions on Tb^{3+}. Our results also reveal that silver particles are responsible for generating deeper capture centers.

1. Introduction

In recent decades, rare earth ions used as activators in different hosts have attracted considerable attention due to their applications in many technological fields, such as conversion materials for solar cells [1], fiber amplifiers [2], solid state lasers [3], radiation detectors [4], photoelectric devices [5] and optical data storage [6]. Moreover, these elements are being used at an increasing rate in different therapeutic and diagnostic applications in modern medicine [7,8].

From the host material point of view, calcium sulfate ($CaSO_4$) polycrystals have received interest as promising phosphors for measuring the ionizing radiation dosimetry by thermoluminescence [9–11] and optically stimulated luminescence techniques [12–14]. Other potential applications of these phosphors for novel display devices include liquid crystal display backlighting and light emitting diodes [15].

In addition to exhibiting good luminescence properties, $CaSO_4$ phosphors have excellent biocompatibility and higher dissolution rates, as well as being biodegradable, thereby making them suitable materials for drug release and artificial tissue development for clinical applications of bone transplantation [16].

In recent years, several studies have been carried out that investigate terbium ion-activated $CaSO_4$ hosts as luminescent materials [17–19]. Consideration has also been given to the use of silver as a co-dopant to improve the luminescent properties of these materials. Co-doping with terbium and silver has been reported as one of the most efficient strategies in increasing the emission intensity of $CaSO_4$ hosts [20,21].

Due to the above-mentioned reasons, the present work is a continuation of an experimental cycle [22], with the purpose of consolidating and enriching our knowledge regarding the structural and luminescent properties of Ag-activated $CaSO_4$:Tb. We employ characterization techniques that include X-ray diffraction (XRD) and photoluminescence (PL) under vacuum ultraviolet (VUV), ultraviolet (UV) and X-ray excited optical luminescence (XEOL) for the analysis of the investigated

* Corresponding author.
E-mail address: dnsouza@academico.ufs.br (D.N. Souza).

https://doi.org/10.1016/j.optmat.2020.110717
Received 1 September 2020; Received in revised form 13 November 2020; Accepted 2 December 2020
Available online 9 December 2020

materials.

2. Material and methods

2.1. Sample preparation

By means of a slow evaporation route, improved by Junot et al. [23], $CaSO_4$:Tb,Ag and $CaSO_4$:Tb,Ag nanoparticle (NP) crystals were produced. The production process was based on a mixture of calcium carbonate ($CaCO_3$) (Merck, 99%), sulfuric acid (H_2SO_4) (Vetec, 95–99%), terbium oxide (Tb_4O_7) (Alfa Aesar, 99.9%) and silver oxide (Ag_2O) (Sigma-Aldrich, 99%) or Ag NPs for co-doped samples. The Ag NPs were prepared through the synthesis process proposed by Lee and Meisel [24], which is based on the chemical reduction of Ag ions ($AgNO_3$) (Neon, 99.8%) using sodium citrate ($Na_3C_6H_5O_7.2H_2O$) (Neon, 99.6%) as a reducing and stabilizing agent. The Tb^{3+} concentration was fixed at 0.1 mol.%, while different amounts of Ag were added to produce a series of samples with the composition range $CaSO_4:Tb_{0.001}Ag_x$, where x = 0.0001, 0.0005, or 0.001.

First, for each material, stoichiometric concentrations were kept under stirring and heated (≈120 °C) until complete homogenization and evaporation of water. The resulting solution was then introduced into a volumetric flask and placed on a heating blanket at 375 °C until all the acid evaporated. Subsequently, the crystals adhered to the wall of the flask were extracted by passing through a series of washes with distilled water at room temperature, followed by washing with distilled water heated to 100 °C, alternately, until the solution pH was ~6. The crystals were then macerated and sifted, and used as grains with diameters between 75 and 150 μm. The resulting powder was transferred to alumina crucibles and calcined for 1 h at 600 °C.

2.2. Sample characterization

XRD measurements were performed using a Rigaku diffractometer (RINT 2000/PC) with Cu-Kα radiation and an X-ray tube operating at 40 kV and 30 mA in continuous scanning mode from 20° to 80° in steps of 0.05°/min. The unit cell was illustrated by VESTA software [25]. The PL measurements were acquired with a JASCO FP8600 spectrofluorometer equipped with a 150 W xenon discharge lamp as the excitation source was used.

The other optical characterizations were made at the X-ray absorption fine structure (XAFS2) and toroidal grating monochromator (TGM) beamline at the Brazilian Synchrotron Light Laboratory(LNLS), part of the Brazilian Center for Research in Energy and Materials (CNPEM). VUV measurements were made in ultra-high vacuum conditions (higher than 10^{-7} mbar) at room temperature. Monochromatic photons filtered using a MgF_2 and a quartz window were used for exciting the samples in a range from 4.5 to 10 eV. The emitted light was collected by an optical fiber coupled to the chamber by a vacuum feedthrough and connected to a photomultiplier and monochromator in the range from 200 to 1000 nm.

XEOL spectra were measured using the emission mode in a dark chamber, coupled to a bifurcated optical fiber in an Ocean Optics HR2000 spectrometer. An X-ray absorption near edge structure (XANES) study was also performed to verify the Tb oxidation state in the Tb-doped $CaSO_4$ materials. XANES data were recorded around the Tb L_{III} edge (7515 eV), in fluorescence mode, with a Ge15 detector from Canberra. Both experiments were carried out at room temperature.

3. Results and discussion

3.1. Structural analysis

The XRD analysis of the $CaSO_4$:Tb,Ag and $CaSO_4$:Tb,AgNP phosphors and the standard diffraction pattern of $CaSO_4$ (ICDD 00-037-1496) is shown in Fig. 1. The results reveal that the obtained samples agree with the ICDD 00-037-1496 pattern, with lattice parameters a = 6.9933 Å, b = 7.0017 Å, c = 6.2411 Å and no evidence of secondary phases observed. The unit cell of $CaSO_4$, illustrated in Fig. 2, contains 24 ions. The calcium (Ca^{2+}) cations are bonded by eight oxygen (O^{2-}) ions located in two different positions, represented as O_1 and O_2, while the sulfur (S^{6+}) ion is surrounded by a tetrahedron of four oxygen ions. The inter-planar distances d_{hkl} of the five major peaks at 2θ values of 25.25°, 31.25°, 38.55°, 40.70°, and 48.65° were 3.5242 Å, 2.8599 Å, 2.3335 Å,

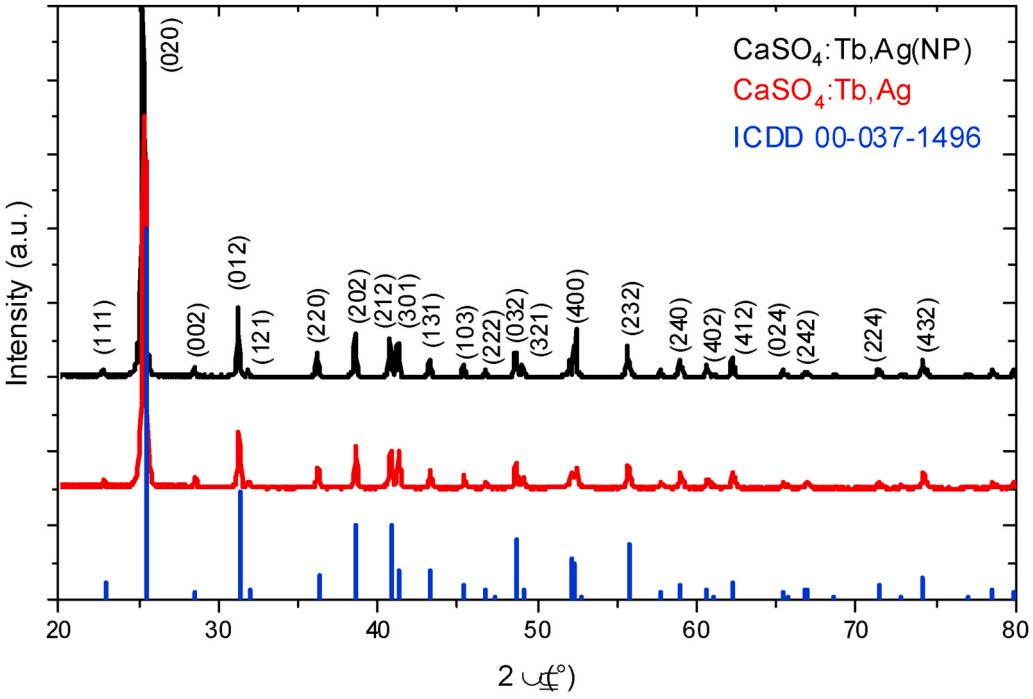

Fig. 1. XRD patterns of $CaSO_4$:Tb,Ag and $CaSO_4$:Tb,Ag(NP) phosphors, in comparison to the pattern (ICDD 00-037-1496). The numbers of each reflection peak are indicated in the figure.

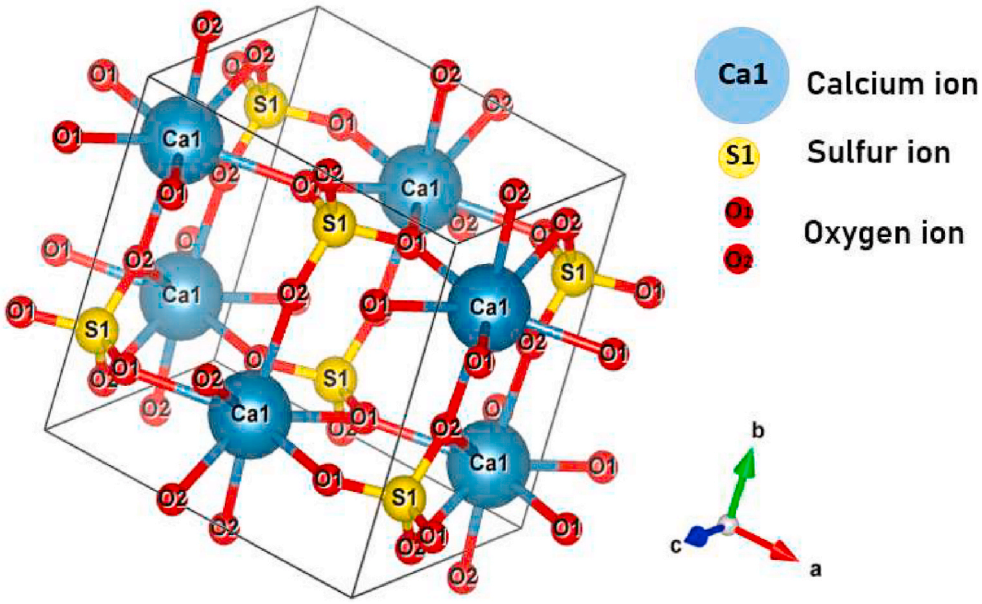

Fig. 2. VESTA representation of $CaSO_4$ unit cell (ICDD 00-037-1496).

2.2150 Å, and 1.8700 Å, respectively. These peaks correspond to the (020), (012), (202), (212), and (032) reflection planes. The lattice parameters of the samples were calculated using the following formula for orthorhombic structure [26]:

$$\frac{1}{d_{hkl}^2}=\frac{h^2}{a^2}+\frac{k^2}{b^2}+\frac{l^2}{c^2}$$

The values of the lattice parameters estimated for the $CaSO_4$: Eu samples are a = 7.0049 Å, b = 7.0484 Å, and c = 6.2581 Å. These experimental values are in strong agreement (less than 0.5% difference) with the pattern of the lattice parameter values.

The low concentrations of dopant ions do not provide easy determination for ion substitution. Generally, the radii difference between the two cations primarily determines whether the doped ions can substitute for the host cation. Since the ionic radius values of Tb^{3+} and Ca^{2+} ions are similar, one may expect that Tb^{3+} ions would occupy the Ca^{2+}

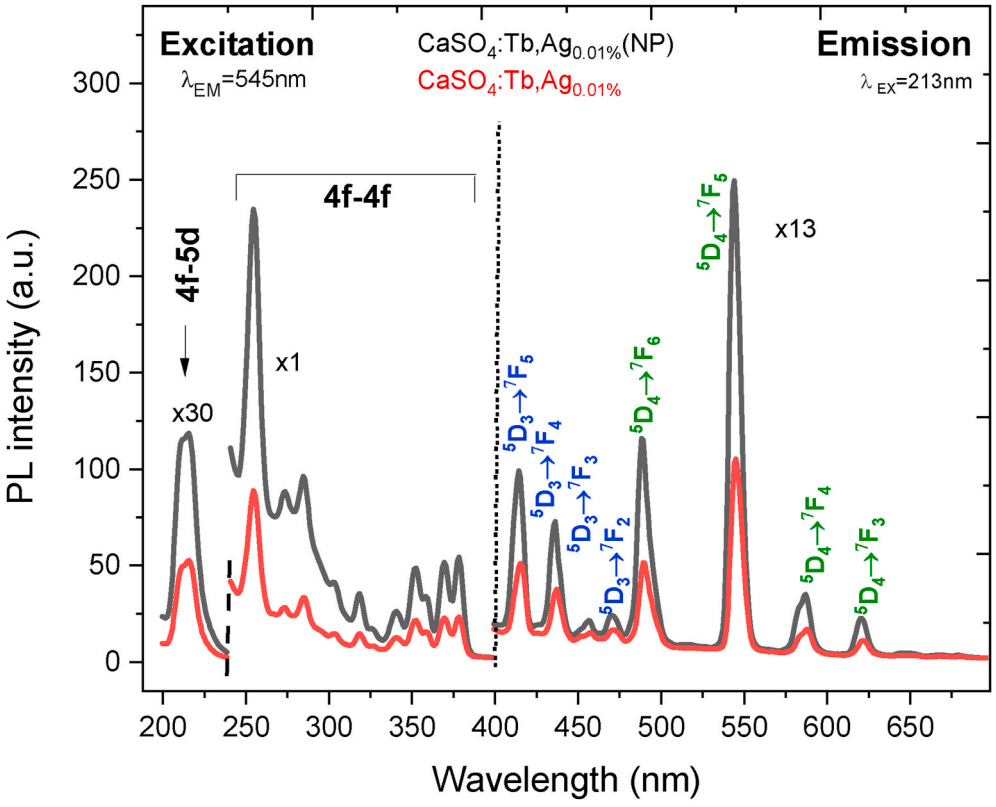

Fig. 3. PL emission and excitation spectrum of (a) $CaSO_4$:Tb,Ag and (b) $CaSO_4$:Tb, AgNP. The symbol x denotes that the intensities are multiplied by the numbers indicated in the spectrum.

site in the lattice. Previous atomistic simulation work [27] has revealed that Eu^{3+} dopant, with similar ionic radii of Tb^{3+} ions, prefers to be incorporated at the Ca^{2+} site with charge compensation by O_i' interstitial defect.

3.2. PL studies

The excitation and emission spectra of the $CaSO_4$:Tb,AgNP and $CaSO_4$:Tb,Ag materials are showed in Fig. 3. The excitation spectra of both samples exhibit a similar profile with a broad absorption band ranging from 200 to 240 nm, with the maximum at ~213 nm attributed to the 4f-5d spin-allowed transition of Tb^{3+}. Weak absorption bands in the region from 240 to 350 nm are also observed, which are ascribed to the 4f-4f transitions of Tb^{3+} [28]. The emission spectra from the samples excited at 213 nm of UV light show the well-known blue-green emission lines due to the Tb^{3+} transitions. The emission lines with maxima at 382, 416, 437.5, 456 and 472 nm are assigned to the $^5D_3 \rightarrow {}^7F_J$ (J = 2, 3, 4 and 5) transitions, while the other peaks at 490, 548, 589 and 622 nm are attributed to the sharp $^5D_4 \rightarrow {}^7F_J$ (J = 6, 5, 4 and 3) transitions, respectively [28,29]. The more intense emission ($^5D_4 \rightarrow {}^7F_5$) at 545 nm is assigned to a magnetic dipole transition with $\Delta J = 1$ [30].

An improvement in the PL emission intensity is found when the sample is doped with Ag NPs. This was attributed to the increased absorption and energy transfer from the host to Tb^{3+} ions in the presence of Ag NPs. The NPs were able to generate structural defects more readily compared with the materials with silver oxide. A similar behavior has been reported for the thermoluminescent emission of this couple of samples [22], which may strengthen this hypothesis.

The integrated PL emission intensities of $CaSO_4$:Tb,Ag and $CaSO_4$:Tb,AgNP as a function of Ag concentration are shown in Fig. 4. It was found that the PL emission intensity of Tb^{3+} increased with higher Ag oxide concentrations and decreased with higher Ag NP concentrations. The PL intensity is higher for materials with 0.01 mol.% Ag NPs and 0.1 mol% Ag oxide. For the $CaSO_4$:Tb,Ag material, this behavior is attributed to local field enhancement effects on the absorption and emission of Tb ions or energy transfer from metallic silver to rare earth ions. In the presence of Ag NPs, the quenching effect is due to the energy transfer from ions to the Ag NPs [31]. This behavior is similar to that observed in the work of Zeferino et al. [32], where a reduction in the UV emission intensity was observed due to interstitial Ag atoms in the ZnO lattice, which created a large amount of defects.

3.3. XEOL and XANES

XEOL emission spectra of the $CaSO_4$:Tb,Ag and $CaSO_4$:Tb,AgNP samples excited at the Tb L_{III}–edge (7.515 eV) are shown in Fig. 5. The spectrum shows typical Tb emissions with twelve lines attributed to the $^5D_3 \rightarrow {}^7F_J$ (J = 6-2) and $^5D_4 \rightarrow {}^7F_J$ (J = 6-0) transitions [33]. The most intense emission peak was located at ~540 nm, which is due to the $^5D_4 \rightarrow {}^7F_5$ transition. In addition, it was possible to observe that the Ag NPs contributed to an increase in the luminescent intensity. This result proves the good stability of $CaSO_4$, since the energy transfer from the defects to the terbium ion when subjected to excitation at high energies is observed.

The integrated XEOL as a function of excitation energy are shown in Fig. 6. It was observed that the XEOL emission tends to decrease as the energy of the excitation photon increases, thus indicating that much of the electron-hole pair recombination process occurs by non-radioactive pathways, which may cause a reduction in the energy transfer phenomenon [34].

The investigation of the valence of the dopants is of great importance, as it can directly influence several optical properties, such as the region and the intensity of the material's luminescent emission. To verify the terbium valence state, X-ray absorption measurements near the edge (XANES) were performed for the samples of $CaSO_4$:Tb,Ag and $CaSO_4$:Tb,AgNP and are shown in Fig. 7(a). The first derivative of the XANES curves are shown in Fig. 7(b). The XANES results for the two samples revealed an intense maximum of ~7515 eV, which, when

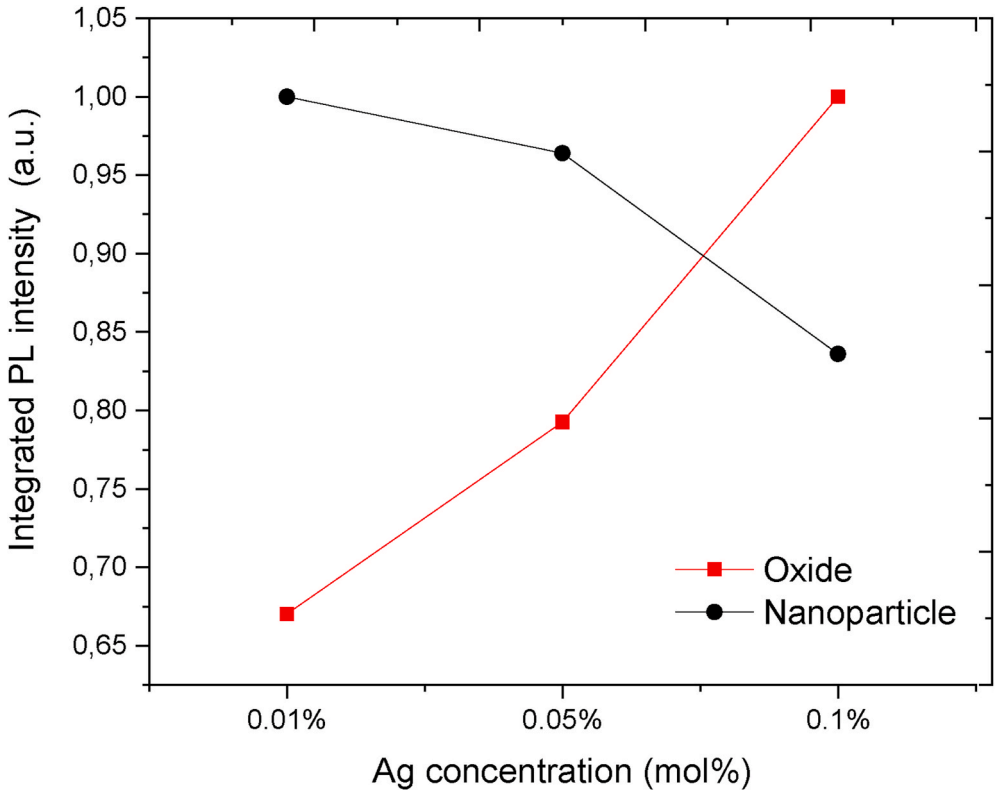

Fig. 4. Integrated PL intensity normalized for $CaSO_4$:Tb,Ag and $CaSO_4$:Tb,AgNP peaks as a function of Ag concentration.

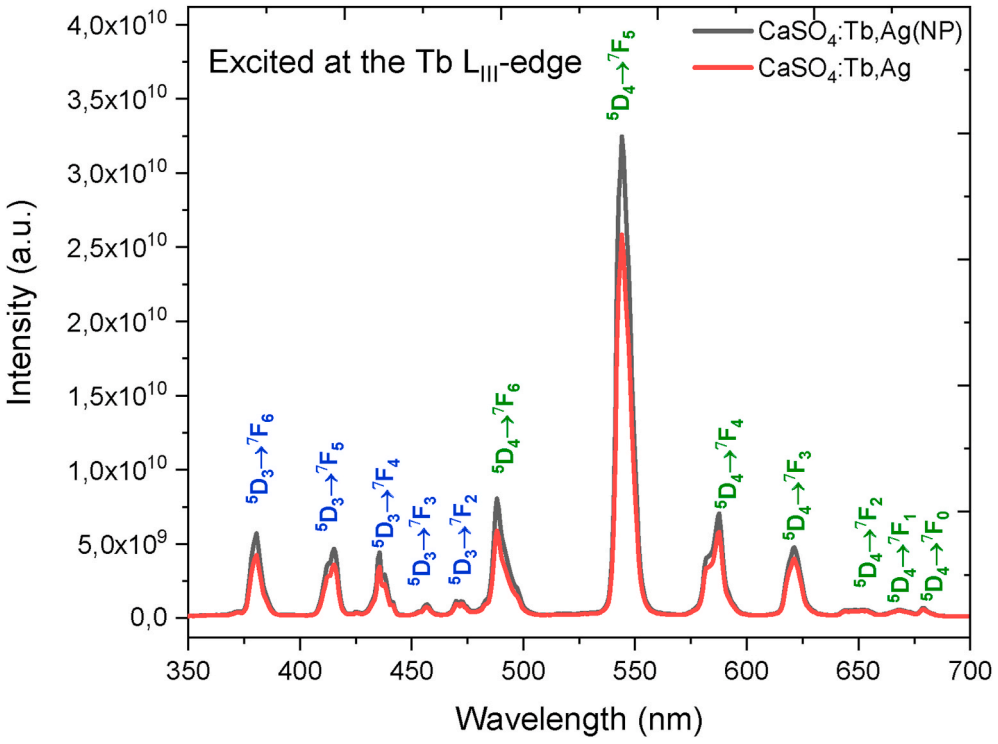

Fig. 5. XEOL emission spectra of Tb and Ag co-doped $CaSO_4$ excited at the Tb L_{III}-edge (7.515 eV).

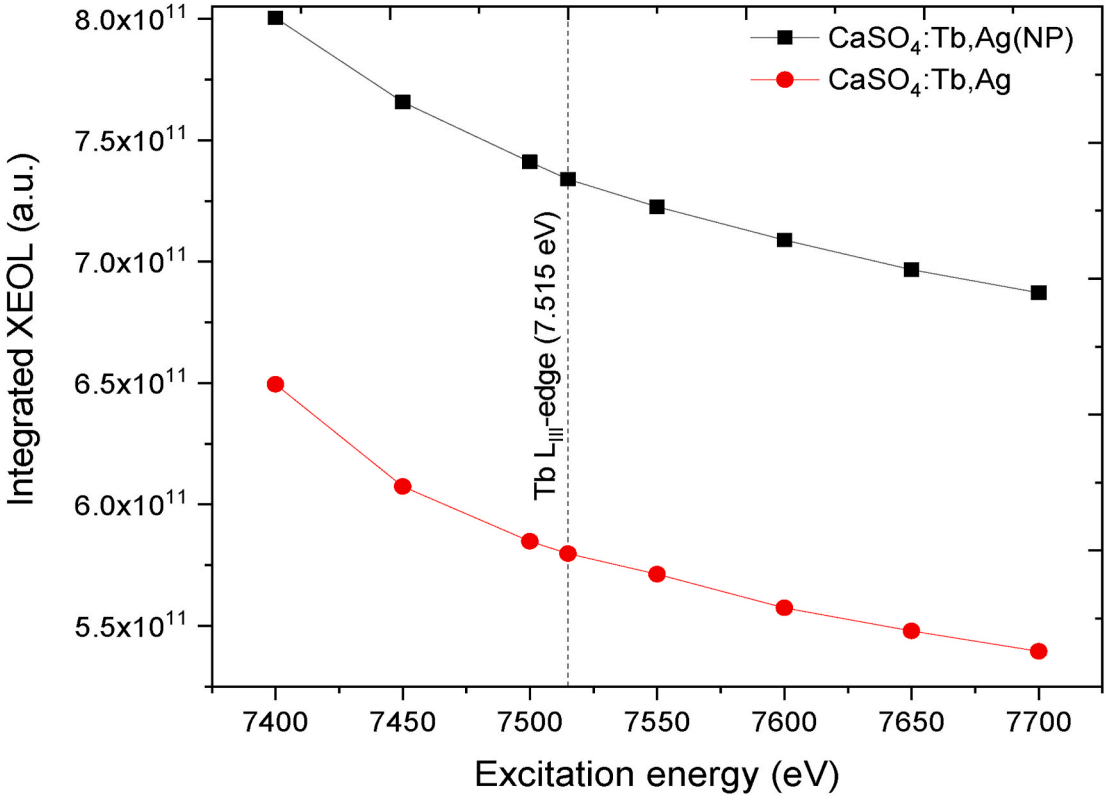

Fig. 6. Integrated XEOL spectra as a function of excitation energy of $CaSO_4$:Tb,Ag and $CaSO_4$:Tb,AgNP samples.

compared to the standard, indicates the predominance of Tb^{3+} ions. As noted, the reference spectrum has two peaks associated with the Tb^{3+} and Tb^{4+} valence states, confirming that there is no evidence of the presence of another oxidation state of Tb in the evaluated samples, such as 4+, which usually manifests itself in the shape of a shoulder next to the maximum [35,36]. This result demonstrated that the addition of silver and exposure to high energies did not influence the valence of terbium.

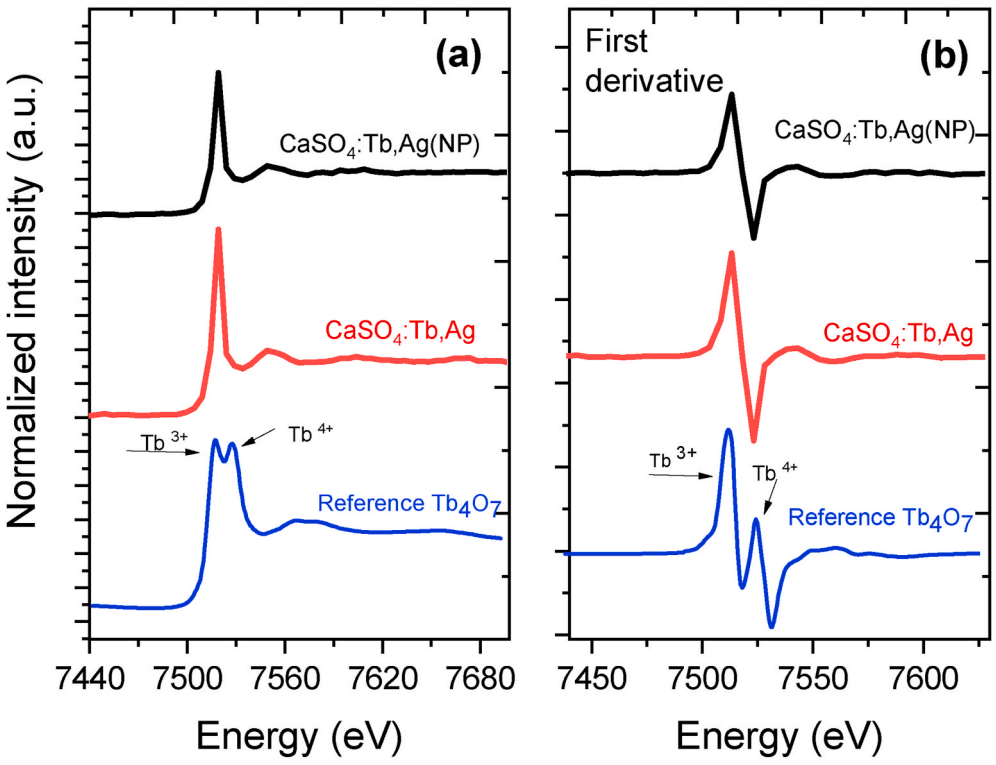

Fig. 7. (a) XANES spectra of $CaSO_4$:Tb,Ag and $CaSO_4$:Tb,AgNP excited at Tb L_{III} -edge. (b) First derivative of XANES spectra.

3.4. VUV spectra

The VUV excitation spectra of the $CaSO_4$:Tb,Ag and $CaSO_4$:Tb,AgNP phosphors measured using synchrotron radiation are shown in Fig. 8. These spectra are composed of three bands: an intense band at 7.6 eV (~163 nm) and two less intense bands at 6.3 eV (~180 nm) and 5.6 eV (~220 nm). In the range of 6–11 eV (~207–112 nm), the bands of host-lattice absorption are characterized. The results indicated that the $CaSO_4$:Tb,Ag phosphor has a larger absorption under the VUV excitation than the $CaSO_4$:Tb,AgNP. The band at 5.0–5.9 eV (210–247 nm) is assigned to the transition from the $^7F_6$ ground state to the ^7D_J excited state, which corresponds to the $4f^8$ to $4f^75d^1$ levels [17]. The peaks from 6 to 9 eV (137–206 nm) are attributed to excitations of the $(SO_4)^{2-}$ complex [37].

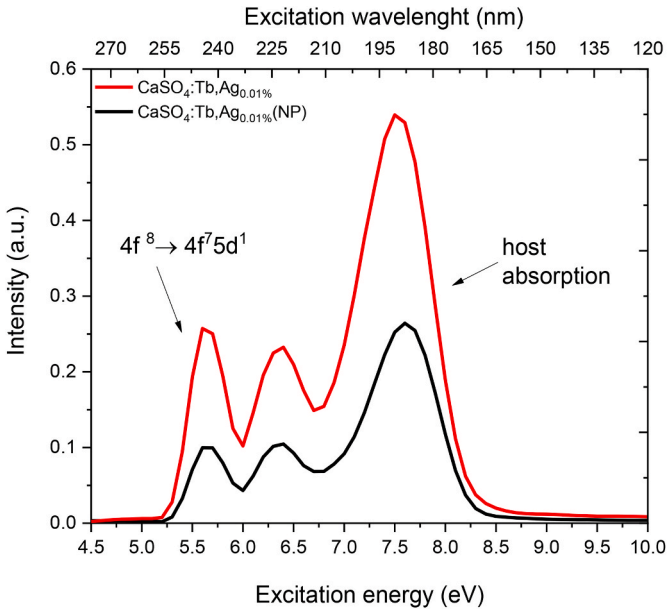

Fig. 8. Excitation spectra of $CaSO_4$:Tb,Ag and $CaSO_4$:Tb,AgNP samples.

To analyze the spectra of the studied materials, isometric graphs in three dimensions, where x, y and z axes represent the excitation energy (eV), wavelength (nm) and intensity (a. u.), respectively, are shown in Figs. 9 and 10. The emissions identified are located at 379, 413, 435, 456, 470, 488, 544, 587 and 620 nm, and that at 544 nm is dominant. These results agree with the emissions previous performed with UV light and X-ray excitation. The emissions in the green region and the emissions in the blue region are attributed to the Tb^{3+} transitions $^5D_4 \rightarrow {}^7F_J$ (J = 6, 5, 4, 3 and 2) and $^5D_3 \rightarrow {}^7F_J$ (J = 6, 5, 4 and 3), respectively.

4. Conclusions

$CaSO_4$:Tb,AgNP and $CaSO_4$:Tb,Ag phosphors were efficiently produced by a slow evaporation route, since the XRD results presented a single phase in agreement with the ICDD 00-037-1496 pattern.

The PL results demonstrate that under excitation with UV light, the Ag NPs influence the spectroscopic properties of Tb-doped $CaSO_4$ crystals, resulting in a significant increase in luminescent intensity. This means that the Ag NPs could contribute to generate structural defects in the lattice. The results also revealed that PL emission intensity of Tb^{3+} increased with higher Ag oxide concentrations used as start reagent and decreased with higher Ag NP concentrations.

Under hard X-ray irradiation at high energies, the XEOL emission spectra show exclusively Tb emission with peaks arising from $^5D_3 \rightarrow {}^7F_J$ (J = 6 - 2) and $^5D_4 \rightarrow {}^7F_J$ (J = 6-0) transitions and the most intense peak located at ~540 nm. The XANES data of the materials indicated the presence of the terbium ion in the trivalent state.

The synchrotron radiation measurements revealed, after the host excitation in the VUV region, three broad bands in the 140–240 nm region with intense host absorption at 5.6, 6.3 and 7.6 eV. All VUV emissions identified are attributed to the transitions of Tb^{3+}. The experiments provide necessary research for the practical application of $CaSO_4$:Tb,Ag and $CaSO_4$:Tb,AgNP blue-green phosphors.

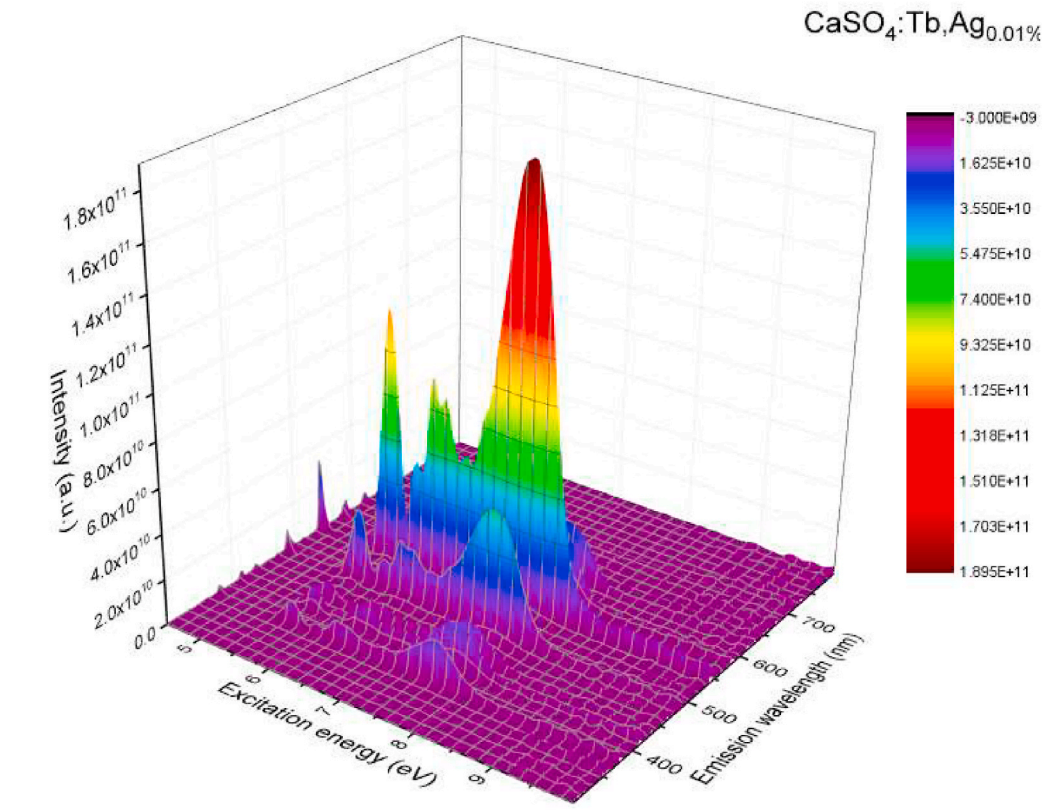

Fig. 9. 3D emission/excitation spectra of $CaSO_4$:Tb,Ag samples.

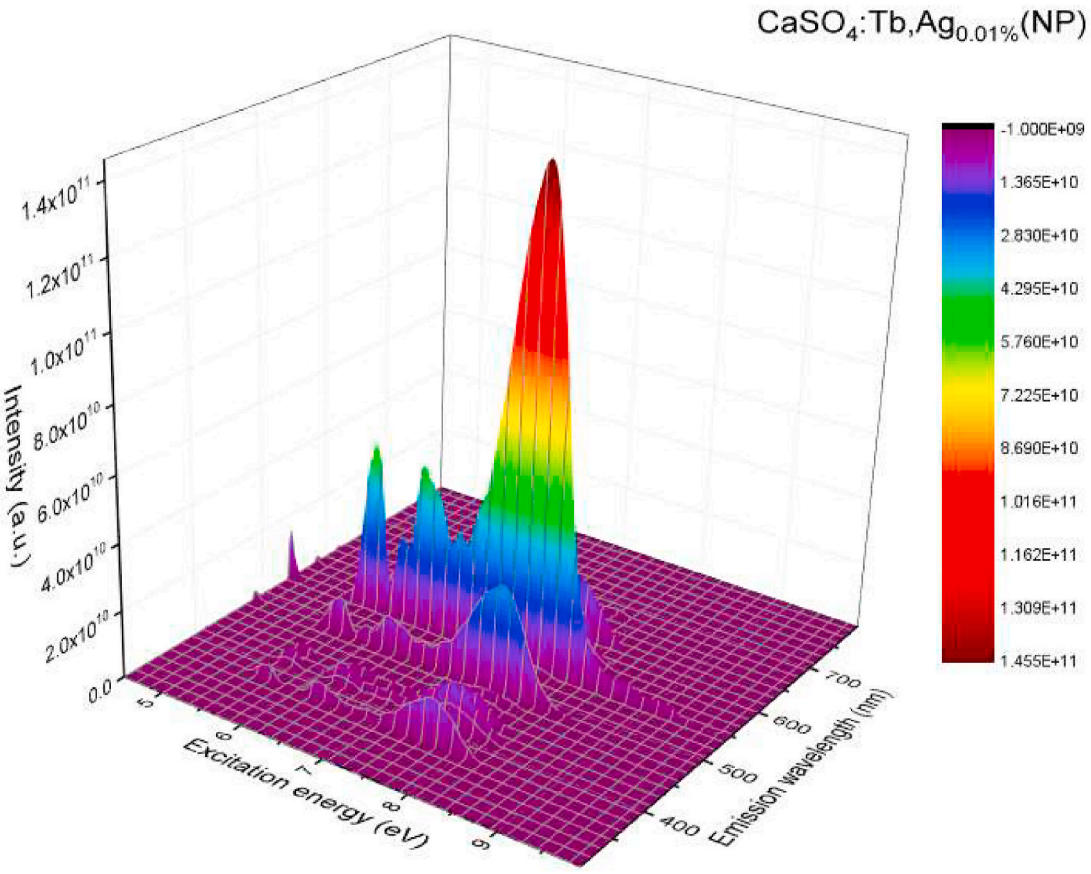

Fig. 10. 3D emission/excitation spectra of $CaSO_4$:Tb,AgNP samples.

CRediT authorship contribution statement

Anderson M.B. Silva: Conceptualization, Methodology, Investigation, Writing - original draft. **Wellisson S. Silveira:** Visualization, Investigation. **Tawany S. Matos:** Investigation. **Danilo O. Junot:** Data curation, Investigation, Validation. **Marcos V.S. Rezende:** Visualization, Resources, Supervision. **Divanizia N. Souza:** Supervision, Resources, Writing - original draft, Project administration.

Declaration of competing interest

The authors declare that they have no known competing financial interests or personal relationships that could have appeared to influence the work reported in this paper.

Acknowledgments

The authors thank the Brazilian Agencies CNEN, CNPq and CAPES for their partial financial support. This research also used resources of the Brazilian Synchrotron Light Laboratory and the TGM and XAFS2 beamline staff for their valuable help on the measurements in the internal research proposal number 20190163.

References

[1] F. Zhao, Y. Liang, J.B. Lee, S.J. Hwang, Applications of rare earth Tb^{3+}-Yb^{3+} co-doped down-conversion materials for solar cells, Mater. Sci. Eng. B 248 (2019) 114404, https://doi.org/10.1016/j.mseb.2019.114404.

[2] S. Tanabe, Optical properties and local structure of rare-earth-doped amplifier for broadband telecommunication, J. Alloys Compd. 408 (2006) 675–679, https://doi.org/10.1016/j.jallcom.2005.01.106.

[3] K. Petermann, G. Huber, L. Fornasiero, S. Kuch, E. Mix, V. Peters, S.A. Basun, Rare-earth-doped sesquioxides, J. Lumin. 87 (2000) 973–975, https://doi.org/10.1016/S0022-2313(99)00497-4.

[4] L.F. Souza, A.M.B. Silva, P.L. Antonio, L.V.E. Caldas, S.O. Souza, F. d'Errico, D. N. Souza, Dosimetric properties of MgB_4O_7:Dy,Li and MgB_4O_7: Ce, Li for optically stimulated luminescence applications, Radiat. Meas 106 (2017) 196–199, https://doi.org/10.1016/j.radmeas.2017.02.009.

[5] Y. Zhuang, L. Wang, L.Y. Lv, T.L. Zhou, R.J. Xie, Optical data storage and multicolor emission readout on flexible films using deep-trap persistent luminescence materials, Adv. Funct. Mater. 28 (2018) 1705769, https://doi.org/10.1002/adfm.201705769.

[6] B.S. Ham, M.S. Shahriar, M.K. Kim, P.R. Hemmer, Frequency-selective time-domain optical data storage by electromagnetically induced transparency in a rare-earth-doped solid, Opt. Lett. 22 (1997) 1849–1851, https://doi.org/10.1364/OL.22.001849.

[7] Y. Chen, Z. Xu, C. Smith, J. Sankar, Recent advances on the development of magnesium alloys for biodegradable implants, Acta Biomater. 10 (2014) 4561–4573, https://doi.org/10.1016/j.actbio.2014.07.005.

[8] T. Wakabayashi, A. Ymamoto, A. Kazaana, Y. Nakano, Y. Nojiri, M. Kashiwazaki, Antibacterial, antifungal and nematicidal activities of rare earth ions, Biol. Trace Elem. Res. 174 (2016) 464–470, https://doi.org/10.1007/s12011-016-0727-y.

[9] L.A. Forner, C. Viccari, P. Nicolucci, Dosimetric properties of thermoluminescent pellets of CaSO4 doped with rare earths at low doses, Radiat. Phys. Chem. 171 (2020) 108704, https://doi.org/10.1016/j.radphyschem.2020 108704.

[10] S.D.S. Fernandez, R. García-Salcedo, J.G. Mendoza, D. Sánchez-Guzmán, G. R. Rodríguez, E. Gaona, T.R. Montalvo, Thermoluminescent characteristics of LiF: Mg,Cu,P and $CaSO_4$: Dy for low dose measurement, Appl. Radiat. Isot. 111 (2016) 50–55, https://doi.org/10.1016/j.apradiso.2016.02.011.

[11] M. Yüksel, T. Dogan, Z.G. Portakal, M. Topaksu, Synthesis and luminescence characterization of microcrystalline Nd-doped calcium sulfate, Appl. Radiat. Isot. 148 (2019) 197–203, https://doi.org/10.1016/j.apradiso.2019.04.005.

[12] S.K. Omanwar, C.B. Palan, Synthesis and preliminary OSL studies of Ce^{3+} activated calcium sulfate ($CaSO_4$) for radiation dosimetry, J. Mater. Sci. Mater. Electron. 29 (2018) 7388–7392, https://doi.org/10.1007/s10854-018-8728-6.

[13] V. Guckan, V. Altunal, N. Nur, T. Depci, A. Ozdemir, K. Kurt, Z. Yegingil, Studying $CaSO_4$: Eu as an OSL phosphor, Nucl. Instrum. Meth. Phys. 407 (2017) 145–154, https://doi.org/10.1016/j.nimb.2017.06.010.

[14] S. Bahl, V. Kumar, R.R. Bihari, P. Kumar, Investigations of OSL properties of $CaSO_4$: Mn phosphor exposed to gamma and beta radiations, J. Lumin. 181 (2017) 36–43, https://doi.org/10.1016/j.jlumin.2016.09.004.

[15] A. Lakshmanan, S.B. Kim, B.G. Kum, H.M. Jang, B.K. Kang, Rare earth doped $CaSO_4$ luminescence phosphors for applications in novel displays–new recipes, Phys. Status Solidi 203 (2006) 565–577, https://doi.org/10.1002/pssa.200521159.

[16] M.V. Thomas, D.A. Puleo, Calcium sulfate: properties and clinical applications, J. Biomed. Mater. Res. B Appl. Biomater. 88 (2009) 597–610, https://doi.org/10.1002/jbm.b.31269.

[17] A. Lushchik, C. Lushchik, I. Kudryavtseva, A. Maaroos, V. Nagirnyi, F. Savikhin, Resonant processes causing photon multiplication in $CaSO_4$: Tb^{3+}, Radiat. Meas. 56 (2013) 139–142, https://doi.org/10.1016/j.radmeas.2013.01.037.

[18] I. Kudryavtseva, A. Lushchik, C. Lushchik, A. Maaroos, V. Nagirnyi, S. Pazylbek, E. Vasil'chenko, Complex terbium luminescence centers in spectral transformers based on $CaSO_4$, Phys. Solid State 57 (2015) 2191–2201, https://doi.org/10.1134/S1063783415110219.

[19] I. Kudryavtseva, A. Lushchik, A. Maaroos, Z. Azmaganbetova, T. Nurakhmetov, Z. Salikhoja, Recombination luminescence of $CaSO_4$:Tb^{3+} and $CaSO_4$: Gd^{3+} phosphors, Open Phys. 10 (2012) 995–1001, https://doi.org/10.2478/s11534-011-0091-7.

[20] U. Madhusoodanan, M.T. Jose, A. Tomita, A.R. Lakshmanan, New thermostimulated luminescence phosphors based on $CaSO_4$:Ag,RE, J. Lumin. 87 (2000) 1300–1302, https://doi.org/10.1016/S0022-2313(99)00598-0.

[21] D.O. Junot, J.J. Rodrigues Jr., D.N. Souza, M.C. Dos Santos, L.A.O. Nunes, The $CaSO_4$: Eu–Ag composite material: thermo-photoluminescence Study, Radiat. Meas. 70 (2014) 1–4, https://doi.org/10.1016/j.radmeas.2014.08.009.

[22] A.M.B. Silva, D.O. Junot, L.V.E. Caldas, D.N. Souza, Structural, optical and dosimetric characterization of CaSO4:Tb, CaSO4:Tb, Ag and CaSO4:Tb,Ag(NP), J. Lumin. 224 (2020) 117286, https://doi.org/10.1016/j.jlumin.2020.117286.

[23] D.O. Junot, J.P. Barros, L.V.E. Caldas, D.N. Souza, Thermoluminescent analysis of CaSO4:Tb,Eu crystal powder for dosimetric purposes, Radiat, Meas 90 (2016) 228–232, https://doi.org/10.1016/j.radmeas.2016.01.020.

[24] P.C. Lee, D. Meisel, Adsorption and surface-enhanced Raman of dyes on silver and gold sols, J. Phys. Chem. 86 (1982) 3391–3395, https://doi.org/10.1021/j100214a025.

[25] K. Momma, F. Izumi, VESTA: a three-dimensional visualization system for electronic and structural analysis, J. Appl. Crystallogr. 41 (2008) 653–658, https://doi.org/10.1107/S0021889808012016.

[26] R. Das, K. Gupta, K. Jana, A. Nayak, U.C. Ghosh, Preparation, characterization and dielectric, ac conductivity with electrochemical behavior of strontium zirconate, Adv. Mater. Lett. 7 (2016) 646–651, https://doi.org/10.5185/amlett.2016.6294.

[27] A.M. Otsuka, D.O. Junot, H. Lima, M.D.S. Rezende, M.C. Santos, Atomistic simulation and spectroscopic study of the Eu3+ doped CaSO4 crystal, J. Lumin. 226 (2020), https://doi.org/10.1016/j.jlumin.2020.117503 117503.

[28] M. Li, L. Wang, W. Ran, Z. Deng, J. Shi, C. Ren, Tunable luminescence inSr ^{2}MgSi$_2$O7: Tb3þ, Eu3þ phosphors based on energy transfer, Materials 10 (2017) 227, https://doi.org/10.3390/ma10030227.

[29] Z. Hao, J. Zhang, X. Zhang, S. Lu, X. Wang, Blue-green-emitting phosphor CaSc2O4: Tb3+: tunable luminescence manipulated by cross-relaxation, J. Electrochem. Soc. 156 (2009) H193, https://doi.org/10.1149/1.3060382.

[30] T. Sheng, Z. Fu, X. Wang, S. Zhou, S. Zhang, Z. Dai, Solvothermal synthesis and luminescence properties of $BaCeF_5$, and $BaCeF_5$: Tb^{3+}, Sm^{3+} nanocrystals: an approach for white light emission, J. Phys. Chem. C 116 (2012) 19597–19603, https://doi.org/10.1021/jp306935k.

[31] O.L. Malta, M.A. Couto dos Santos, Theoretical analysis of the fluorescence yield of rare earth ions in glasses containing small metallic particles, Chem. Phys. Lett. 174 (1990) 13–18, https://doi.org/10.1016/0009-2614(90)85319-8.

[32] R.S. Zeferino, M.B. Flores, U. Pal, Photoluminescence and Raman scattering in Ag-doped ZnO nanoparticles, J. Appl. Phys. 109 (2011), 014308, https://doi.org/10.1063/1.3530631.

[33] F. Heigl, A. Jürgensen, X.T. Zhou, Y.F. Hu, L. Zuin, T.K. Sham, Communication: X-ray excited optical luminescence from $TbCl^3$ at the giant resonance of terbium, J. Chem. Phys. 138 (2013), 061104, https://doi.org/10.1063/1.4792043.

[34] S.M. O'Malley, P. Revesz, A. Kazimirov, A.A. Sirenko, Time-resolved x-ray excited optical luminescence in InGaN/GaN multiple quantum well structures, J. Appl. Phys. 109 (2011) 124906, https://doi.org/10.1063/1.3598137.

[35] H. Arashi, S. Shin, H. Miura, A. Nakashima, M. Ishigame, O. Shimomura, Investigations of valence change of Tb ions in ZrO_2-Tb_4O_7 mixed conductor using XANES measurements, Solid State Ionics 35 (1989) 323–327, https://doi.org/10.1016/0167-2738(89)90316-0.

[36] I.A.A. Terra, L.J. Borrero-González, J.M. Carvalho, M.C. Terrile, M.C.F.C. Felinto, H.F. Brito, L.A.O. Nunes, Spectroscopic properties and quantum cutting in Tb^{3+}–Yb^{3+}co-doped ZrO_2 nanocrystals, J. Appl. Phys. 113 (2013), 073105, https://doi.org/10.1063/1.4792743.

[37] E. Van der Kolk, P. Dorenbos, A.P. Vink, R.C. Perego, C.W.E. Van Eijk, A. R. Lakshmanan, Vacuum ultraviolet excitation and emission properties of Pr^{3+} and Ce^{3+} in MSO_4 (M= Ba, Sr, and Ca) and predicting quantum splitting by Pr^{3+} in oxides and fluorides, Phys. Rev. B 64 (2001) 195129, https://doi.org/10.1103/PhysRevB.64.195129.